ACS APPLIED MATERIALS & INTERFACES

Research Article

www.acsami.org

Ethane Selective IRMOF-8 and Its Significance in Ethane–Ethylene Separation by Adsorption

João Pires,*[,†] Moisés L. Pinto,[‡] and Vipin K. Saini[†,§]

[†]Centro de Química e Bioquímica, Faculdade de Ciências, Universidade de Lisboa, 1749-016 Lisboa, Portugal

[‡]Department of Chemistry, CICECO, University of Aveiro, 3810-193 Aveiro, Portugal

Supporting Information

ABSTRACT: The separation of ethylene from ethane is one of the most energy-intensive single distillations practiced. This separation could be alternatively made by an adsorption process if the adsorbent would preferentially adsorb ethane over ethylene. Materials that exhibit this feature are scarce. Here, we report the case of a metal–organic framework, the IRMOF-8, for which the adsorption isotherms of ethane and ethylene were measured at 298 and 318 K up to pressures of 1000 kPa. Separation of ethane/ethylene mixtures was achieved in flow experiments using a IRMOF-8 filled column. The interaction of gas molecules with the surface of IRMOF-8 was explored using density functional theory (DFT) methods. We show both experimentally and computationally that, as a result of the difference in the interaction energies of ethane and ethylene in IRMOF-8, this material presents the preferential adsorption of ethane over ethylene. The results obtained in this study suggest that MOFs with ligands exhibiting high aromaticity character are prone to adsorb ethane preferably over ethylene.

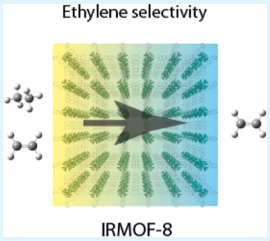

KEYWORDS: *adsorption, porous materials, metal–organic framework, ethane, ethylene, IRMOF-8*

1. INTRODUCTION

Short-chain unsaturated hydrocarbons such as propylene or ethylene have major importance in petrochemical industry. They are common building blocks for plastics, and, by the year 2000, nearly 50 million tones/year of polyethylene were produced worldwide.[1] In an ethylene production plant, when ethylene is to be deethanized, the feed mixture is already essentially ethane and ethylene without significant contaminations.[2] The separation of ethylene from ethane is made by cryogenic distillation. An example of the ethane/ethylene ratio in the mixture is 1:1 (volume) in the refinery off-gas composition.[3] It is important to have in mind that 75–85% of the ethylene costs are due to the high energy consumption that is needed to separate it from ethane,[4] being one of the most energy-intensive single distillations practiced commercially. Adsorption processes are serious candidates for the separation of ethylene from ethane, and various selective adsorbents for this separation exist.[5,6] Nevertheless, the use of adsorption is still not economically viable, the main reason being related to the adsorption operation process.[7,8] Most of the known adsorbents display preferential adsorption of ethylene over ethane. This implies an additional desorption step, normally using an inert gas or applying vacuum, to obtain the high-purity ethylene required in the petrochemical industry, which complicates the technology of the process, making its implementation difficult due to economic reasons.[7−9] Therefore, if the alkane is preferentially adsorbed, pure alkene is directly obtained during the adsorption step, and the whole separation scheme becomes much simpler.[8,9] In this way, major breakthroughs in this field are related to the discovery of adsorbents that present preferential adsorption of ethane over ethylene. Few materials[10,11] or simulaton studies[12,13] showed the possibility of preferential ethane adsorption. Recently, in a metal–organic framework (MOF), the imidazolates ZIF-7 and ZIF-8 were reported as materials that present preferential adsorption of ethane over ethylene, due to a gate-opening mechanism.[7,9,14,15]

MOFs are a type of porous coordination polymers, with metal sites and organic linkers, which are presently well-known, and about which a number of recent reviews exist in the literature.[16−20] In this Article, we report the adsorption of ethane and ethylene in the metal–organic framework IRMOF-8. This material has zinc metal centers, and the organic linker is the naphthalene-2,6-dicarboxylate (structure in Figure S1, Supporting Information).[21] IRMOF-8 was chosen because it has relatively small pores in context of MOFs, so important surface–molecule interactions were expected even for relatively small molecules such as ethane and ethylene. The absence of unsaturated metal sites in the structure is also important for ethane/ethylene separation. In fact, unsaturated metal sites would tend to interact strongly with the ethylene double bond, and so the ethylene would be more adsorbed than ethane. Additionally, improvements in the synthesis process of IRMOF-8 have been reported that indicate good prospects for the synthesis scalability and, therefore, for potential applications.[22] We are not presenting here the answer for the separation of ethylene from ethane by adsorption, but we are presenting results that we believe would be a contribution to this field because they enlighten that MOFs, such as IRMOF-8,

Received: February 24, 2014
Accepted: July 10, 2014
Published: July 10, 2014

can display selective adsorption of ethane over ethylene in certain experimental conditions.

Theory. *IAST Selectivity.* The Ideal Adsorbed Solution Theory (IAST) is by far the most used method for estimating adsorbed phase composition and selectivity of adsorbed gas mixtures. In the present work, we followed a method proposed by Myers,[23] whose implementation is detailed in previous works.[24,25] Briefly, the Gibbs free energy of desorption is estimated by an equation of state from the pure gas adsorption isotherms on the solid adsorbent. For this, the adsorption isotherm must be described by an analytical expression and in the present work the virial equation in the form:

$$p = \frac{n^{ads}}{K} \exp(C_1 n^{ads} + C_2 n^{ads^2} + C_3 n^{ads^3}) \quad (1)$$

where K is the Henry constant and C_1, C_2, and C_3 are the respective virial coefficients. The integration of eq 1 will give the free Gibbs energy of desorption, as follows:

$$G = RT \int_0^p \frac{n^{ads}}{p} dp = RT\left(n^{ads} + \frac{1}{2}C_1 n^{ads^2} + \frac{2}{3}C_2 n^{ads^3} + \frac{3}{4}C_3 n^{ads^4}\right) \quad (2)$$

In this equation, the adsorbed amount n^{ads} and the Gibbs free energy G are functions of temperature and pressure, that is, $n(T, p)$ and $G(T, p)$. The composition of the adsorbed and gas phases of mixtures of C_2H_6 and C_2H_4 may be estimated using the IAST and the Gibbs free energy for the pure components (eq 2). This theory assumes that the mixing of the adsorbed phases of the two components is ideal, although activity coefficients may also be estimated from adsorption isotherms of mixtures to account for nonideal behavior. These nonidealities arise mainly due to adsorbate−adsorbate interactions and are often less dominant than adsorbate−adsorbent interactions already accounted for by IAST.

The standard state for forming adsorbed solutions from the pure components is the free Gibbs energy of the pure components. The selectivity values (separation factor), for a given binary gas-phase composition and pressure, can be calculated, at constant pressure and temperature, and assuming the ideal behavior, by the difference in pure-component Gibbs free energy:[26]

$$G_2 - G_1 = RT \int_0^1 \left[\frac{n_1^{ads}}{y_1} - \frac{n_2^{ads}}{y_2}\right] dy_1 \approx \overline{n}^{ads} RT \ln(S_{1,2}) \quad (3)$$

Equation 3 may be used, at high pressures, to estimate the mean selectivity (S) at constant pressure and temperature, by $\ln(S_{1,2}) = G_2 - G_1/\overline{n}^{ads}RT$, were G_1 and G_2 are the Gibbs free energy of components 1 and 2, $\overline{n}^{ads}$ is the mean adsorbed amount, and y_1, y_2 are the molar fractions of components 1 and 2 in the gas phase. The evaluation of the pure component adsorbed amounts ($\overline{n}_1^{ads}$, $\overline{n}_2^{ads}$) must satisfy the condition $p_1(\overline{n}_1^{ads}) = p_2(\overline{n}_2^{ads})$, for constant pressure. This can be achieved by numerically solving eq 1 for a given value of p. Using eq 2, the Gibbs free energies G_1 and G_2 are calculated for the $\overline{n}_1^{ads}$, $\overline{n}_2^{ads}$, respectively, and finally substituted into eq 3 to obtain the mean selectivity coefficients S.[24,25] The detailed procedure for calculating G_1 and G_2 is described elsewhere.[24]

DFT Models. Molecular and electronic structures of the gas molecules and IRMOF-8 material were studied using density functional theory (DFT) methods. The model used for the IRMOF-8 is presented in Figure 1, and includes one linker and two metal clusters. The other linkers in this simplified model were substituted by the acetate groups, meaning that the aromatic rings were replaced by methyl groups. Geometry optimizations have been computed using Gaussian 09 software[27] considering the molecules in the gas phase, using the hybrid functional M06-2X of Truhlar and Zhao[28,29] with the 6-31G(d,p) basis set. This functional was chosen because it has been reported to give accurate results for modeling noncovalent interaction in graphene.[30] London dispersion forces are known to contribute more than 60% to the adsorption of organic molecules, and hybrid functionals, which account for dispersion, give more accurate results as compared to experimental data.[30] Electrostatic potential was calculated from the self-consistent field electron density matrix of the optimized structures.

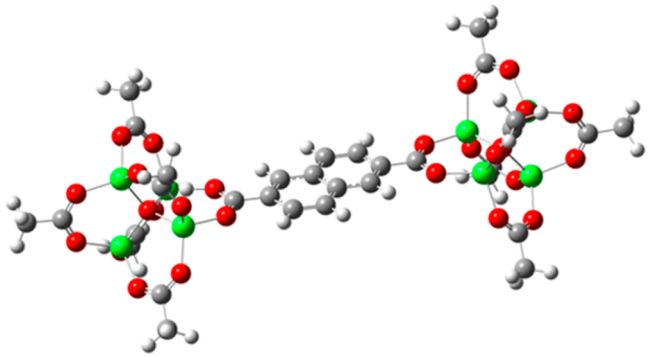

Figure 1. Cluster model of the IRMOF-8 used in the modeling of the systems by DFT ($Zn_8O_{26}C_{32}H_{36}$). Atom types are represented by colors: red, oxygen; gray, carbon; white, hydrogen; green, zinc.

All atoms positions of the IRMOF-8 cluster and gas molecules were optimized using the above-described method. Molecular simulation of the interaction of the ethane and ethylene with the surface cluster was calculated by optimizing only the positions of the atoms of ethane and ethylene and their distance and position relative to the IRMOF-8 cluster, keeping all previously optimized atoms positions of the cluster frozen during this step. A Born−Haber cycle was used to estimate the interaction energy of gas molecules with the IRMOF-8 cluster.

2. EXPERIMENTAL SECTION

Synthesis of IRMOF-8. For the synthesis of IRMOF-8, the following reagents were used: zinc nitrate hexahydrate [$Zn(NO_3)_2 \cdot 6H_2O$, Aldrich, >99%], naphthalene-2,6-dicarboxylic acid, sometimes referred to as 2,6-NDC ($C_{10}H_6(CO_2H)_2$, Aldrich, 99%), and dimethylformamide (DMF, Aldrich, 99.8%). The synthesis procedure was adapted from a previous study.[22] In a 100 mL Pyrex conical flask, a solution of 2.30 g of $Zn(NO_3)_2 \cdot 4H_2O$ (8 mmol) and 0.86 g of 2,6-naphthalene dicarboxylic acid (4 mmol) was prepared in 80 mL of DMF. This solution was sonicated for about 15 min, to obtain a clear solution. This solution was then transferred to a Teflon vessel of autoclave and placed in an oven for synthesis at 393 K, for 20 h. In the end, the autoclave was removed from the oven and allowed to cool to room temperature. Pale yellow crystals of IRMOF-8 were obtained that had settled in the bottom of the yellow supernatant. The yellow supernatant was decanted, and the crystals were washed three times with DMF. For each washing, it was stirred with 25 mL of DMF for 10−15 min, and then separated with centrifuge. After being washed, the crystals were transferred to a Schlenk tube, for further cleaning

(removing solvent) under vacuum at 443 K. The yield was approximately 96% at the optimum synthesis temperature (393 K). The product so obtained was stable in air, and stored under nitrogen.

The diffuse reflectance infrared Fourier transform (DRIFT) spectra of the samples were collected on a Nicolet 6700 at 2 cm^{-1} resolution using the smart diffuse reflectance accessory, at room temperature with a DTGS TEC detector. The samples were prepared by mixing with KBr in an agate mortar. Each collected spectrum was an average of 128 scans of the sample subtracted by the average of 64 background scans using only KBr in the sample container. X-ray diffractograms were obtained by the powder method in a Philips PW 1710 diffractometer, with automatic data acquisition (APD Phillips (v.35B) software) and Cu Kα (λ = 1.5406 Å) radiation. Thermogravimetry experiments were carried out in an apparatus from Setaram (TG-DSC 111), with 0.001 mg of precision, under dry nitrogen flux. For nitrogen adsorption at 77 K, nitrogen (Air Liquid, 99.999%) adsorption isotherms were determined in a volumetric automatic apparatus (Quantachrome, Nova 2200e) at 77 K using a liquid nitrogen cryogenic bath. The sample (between 50 and 100 mg) was degassed for 24 h at a pressure lower than 0.133 Pa and a temperature of 473 K.

Adsorption of Ethane and Ethylene. The adsorption isotherms of ethane (Air Liquide, 99.995%) and ethylene (Matheson, 99.995%) were measured up to a high pressure of 1000 kPa (10 bar), at 298 K. These experiments were carried out on a custom-made volumetric apparatus, made of stainless steel, which is comprised of a pressure transducer (Pfeiffer Vacuum, APR 266) equipped with a vacuum system that allows a vacuum better than 10^{-2} Pa. During experiments, the temperatures were maintained with a stirred thermostatic water bath (Grant Instrument, GD-120), and before every experiment the samples were degassed for 2.5 h at 423 K. The uncertainties in the experimental method, which was estimated by the repeatability of the experiments, were found below 2%. The effect of this maximum value on the calculated selectivity is below 8% and does not have a significant influence on the interpretation of the results.

The adsorption and separation of ethane/ethylene mixtures were performed by the chromatographic method, at 301, 308, and 318 K. The selectivity was determined in a gas chromatograph (Hewlett-Packard, 5890A) by the ratio of the retention times in a 100 mm × 3.2 mm stainless steel tube, using helium (Praxair, 99.999%) as the carrier gas at 20 mL/min and about 80 kPa (mass flow controller; McMillan 80D) and a thermal conductivity detector at 363 K. The column with the IRMOF-8 was prepared with 100 mg of sample powder determined by weighing the column (Mettler, AE240). The column was initially degassed, at 423 K during 2 h, with a helium flow of 30 mL/min. The 50:50 (v/v) hydrocarbon mixture was prepared from ethane (Air Liquide, 99.995%) and ethylene (Matheson, 99.995%). The mixture (3 μL) was manually injected (syringe Hamilton, 7105N) in the gas flow using a standard injection port at the experiment temperature. The retention factor (ratio of the retention times) is a characteristic of a given material and can be faced as a measure of the selectivity of a given separation. In this work, the selectivity (S) of the separation was determined as $S = (t_2 - t_0)/(t_1 - t_0)$, where t_1 and t_2 are the retention times of the first and second peaks of the chromatogram of the mixture and t_0 is the retention time of a nonadsorbing specie (nitrogen in our case) on the column prepared with IRMOF-8. At least two determinations of the retention times were done by repeated injections, and the average selectivity value is reported. The assignment of the peaks was made in some previous experiments with injection of the pure ethane and ethylene, and comparison of the retention times. It was found that ethylene always had smaller retention times than ethane in all studied temperatures.

3. RESULTS AND DISCUSSION

FTIR spectra confirm the main bands of IRMOF-8, the coordination of the naphthalene-2,6-dicarboxylate, and the absence of solvent (dimethylformamide), (Figure S2, Supporting Information, and respective discussion). The absence of solvent is also supported by the thermogravimetric analysis (Figure S3, Supporting Information) that shows a minimum mass loss below 673 K (3.3%). X-ray powder diffraction data (Figure S4, Supporting Information) showed a very good agreement with data previously published.[21,22,31]

The nitrogen adsorption−desorption isotherm at 77 K (Figure 2) shows a type I isotherm, according to the IUPAC

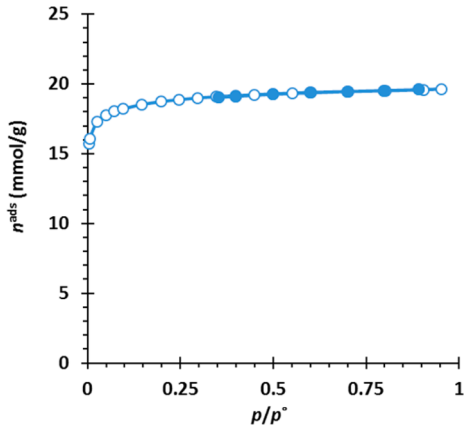

Figure 2. Nitrogen isotherms at 77 K on the IRMOF-8 sample.

classification,[32] characteristic of microporous materials (pore widths less than 2 nm)[27] as expected for the IRMOF-8 structure and in accordance with the literature.[21,22,31] Specific surface area (A_{BET}) was 1360 $m^2\ g^{-1}$ (Langmuir specific surface area was 1887 $m^2\ g^{-1}$), and total pore volume, at p/p^0 = 0.95, was 0.69 $cm^3\ g^{-1}$.

These values are within the range reported in the literature, although some differences can be found among the reported values depending on the synthesis and activation conditions.[21,22,31]

Figure 3 shows the adsorption isotherms of ethane and ethylene on IRMOF-8 at 298 and 318 K for pressures up to 1000 kPa (10 bar), where it can be seen that the ethane adsorbed amounts are higher than those for ethylene in a wide range of pressures, until near 600 kPa. At high pressures, that is, at higher adsorbed amounts, a high number of preferential surface adsorption sites start to be occupied, and the interactions of the molecules are then not only with the surface, but also of the type molecule−molecule. Therefore, at high pressures, the effect of the adsorbent surface is not exerted in the same way as for low and moderate surface coverage, and the adsorbed amounts of ethylene can be higher than for ethane.

The fitting of the virial equation to the adsorption data (Supporting Information, Table S1) allowed one to obtain Henry's constants, which reflect the interaction of the gases with the material in the low pressure limit. The obtained values were significantly higher for ethane than for ethylene at both studied temperatures and quantify the stronger interaction of ethane with the surface. Heats of adsorption were calculated from the adsorption data at the temperatures of 298 and 318 K by the isosteric method (Figure 4). By this methodology, and by convention, the isosteric heats of adsorption are positive. It should be noticed that, although the values in Figure 4 cannot be directly compared to the interaction energy, $U_{interaction}$ (see below), results show that, for low coverage where the interaction with the surface of the material dominates, the energy is higher for ethane than for ethylene, in a similar trend as for the results in sites 1 and 3. The fact that the isosteric heats of ethane are again higher than those for ethylene at high

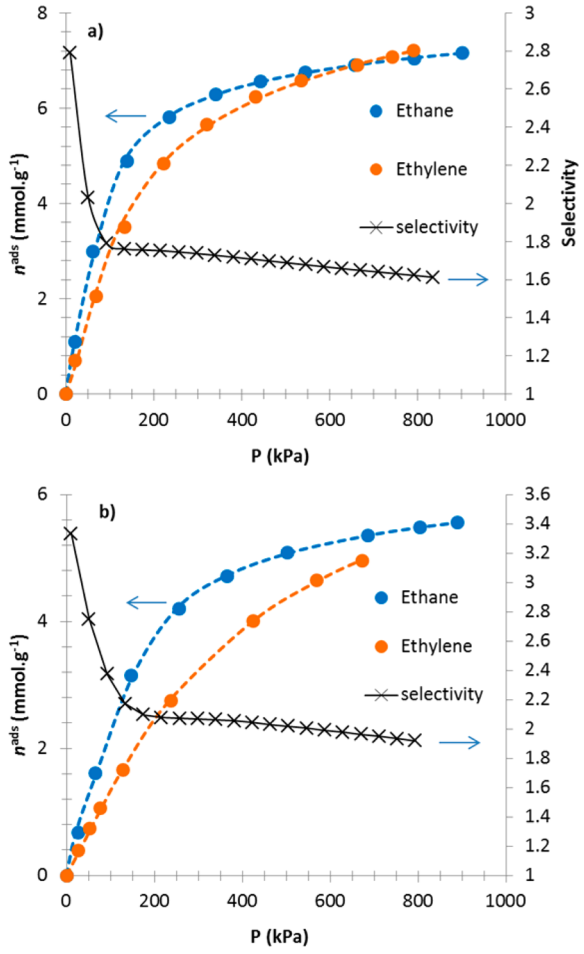

Figure 3. Adsorption isotherms of ethane and ethylene on IRMOF-8 at 298 (a) and 318 K (b), and selectivity values. Lines represent the fit of the virial equation to calculate the selectivity (see Experimental Section).

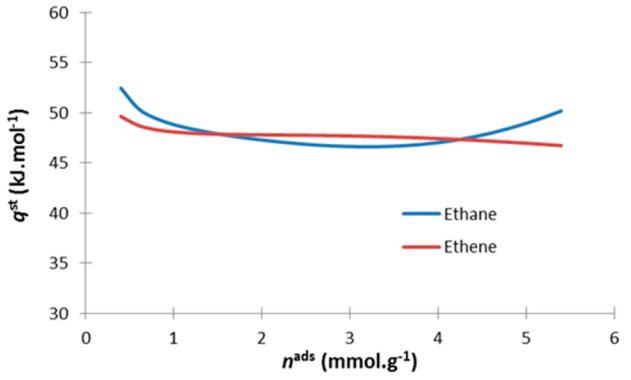

Figure 4. Isosteric heats of adsorption for ethane and ethylene on IRMOF-8.

coverage can be ascribed to a different type of mechanism. In this region, molecule−molecule interactions contribute significantly for the total adsorption heat, and, because the ethane molecule is bulkier, it favors this type of interaction.

In Figure 3, selectivity (or separation factor) values, estimated by a methodology proposed by Myers[23] based on the IAST and detailed above, are given. At 298 K, selectivity has initially a value of 2.8 and decreases with pressure (or adsorbed amounts) until near 1.6. These limits are between 3.4 and 1.9 at 318 K.

The separation of ethylene from ethane was performed in flow experiments in an IRMOF-8 filled column at several temperatures. In initial experiments with just pure component (ethane or ethylene) in the stream, it was found that ethane is always more retained (longer retention times) in the column than ethylene. When mixtures of these hydrocarbons (about 50:50 in volume) are passed in the column, a separation of the two compounds is achieved (Figure 5). The averages of the

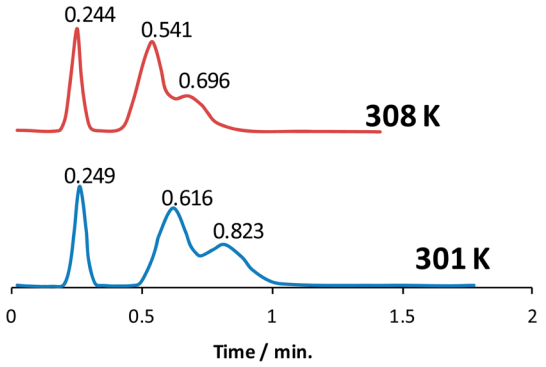

Figure 5. TCD signal obtained at the end of the IRMOF-8 filled column in flow separation of ethane/ethylene mixtures. The first peak (lowest retention time) corresponds to nitrogen, the second to ethylene, and the third to ethane.

adjusted retention times, t' (difference to the nitrogen peak), and of the respective selectivities are favorable to the separation of the ethane/ethylene mixture at all tested temperatures (Table 1), because the column selectively retains more of the

Table 1. Adjusted Retention Times (t') of the Mixture Components on the Column Filled with the IRMOF-8 and the Respective Selectivity, at Different Temperatures

temp/K	t'(ethylene)/min	t'(ethane)/min	selectivity
301	0.372 ± 0.002	0.580 ± 0.002	1.56 ± 0.01
308	0.297 ± 0.001	0.454 ± 0.002	1.53 ± 0.01
318	0.230 ± 0.004	0.329 ± 0.001	1.43 ± 0.03

ethane than the ethylene. This is the expected result considering the equilibrium adsorption isotherms (Figure 3) and indicates that the separation is achieved due to equilibrium with the surface and not due to kinetic effects. Because the experiments were performed at an absolute pressure of 180 kPa, we can consider that the selectivities in Table 1 correspond to selectivities above atmospheric pressure. Comparing the values in Table 1 with those in Figure 3 above 100 kPa, we can conclude that selectivity values are in fair agreement, and support the applicability of the IAST-based method employed in the estimation of the selectivity at several pressures.

It should be noticed that comparison of the selectivity values with literature is limited because, as already mentioned, most of the studies present adsorbents with preferable ethylene adsorption. Nevertheless, estimated selectivity values for MOFs that present preferable ethane adsorption range between 2 and 1.7,[9,14] therefore presenting values near to or slightly below those reported in the present work. It is important to note that some industrial applications exist where the selectivity is between 2 and 3.[6] In our view, the experimental facts

dx.doi.org/10.1021/am502686g | ACS Appl. Mater. Interfaces 2014, 6, 12093−12099

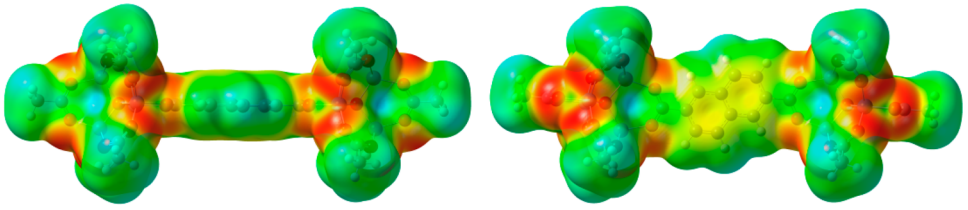

Figure 6. Electrostatic surface potential (ESP) mapping on the electron density surface of the IRMOF-8 cluster. Red regions are negative ESP, and blue regions are positive ESP.

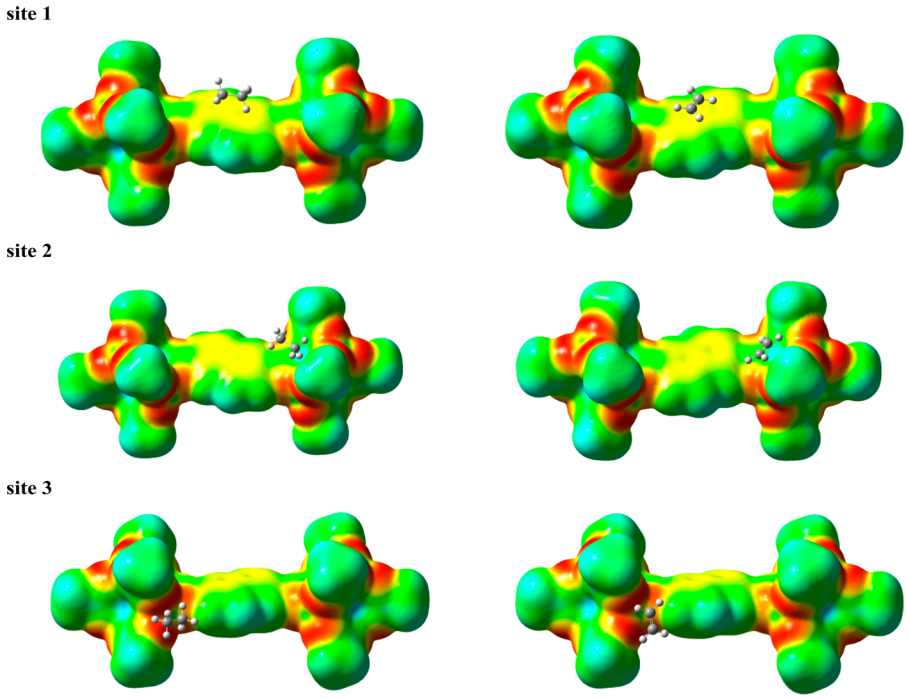

Figure 7. Ethane (left) and ethylene (right) adsorbed on adsorption site 1 with slightly negative ESP zone (yellow), site 2 with positive ESP zone (blue), and site 3 with strong negative ESP zone (red) of the IRMOF-8 cluster. The ESP surface shown was calculated without the presence of the adsorbed molecules (see Figure 6).

illustrated in Figure 3 and Table 1 are due to the differences of interaction between ethylene and ethane with the IRMOF-8 surface.

To understand the differences in the molecular interactions with the surface, a DFT method was used to model the two systems (ethane, IRMOF-8 and ethylene, IRMOF-8). First, to explore where the gas molecules could interact more strongly with the MOF structure, the calculations of the electrostatic surface potential (ESP) on the electron density of the IRMOF-8 cluster chosen to model the material were made. Figure 6 shows that strong negative ESP (red) appears near the corners where the bridging oxygen atoms between the linkers and the zinc centers are located. A less negative ESP (yellow) zone appears over the two aromatic rings. The positive ESP zone (blue) is a spot between the three linkers connected to the metal cluster (i.e., between three ZnO_4 tetrahedra). These positive and negative ESP zones are where the gas molecules could interact more strongly with the IRMOF-8 structure based on electrostatic forces (i.e., noncovalent bonding). Thus, these three sites were chosen as possible adsorption sites to investigate the interaction of the adsorbed molecules with the IRMOF-8 framework.

The equilibrium positions of the ethylene and ethane molecules on the IRMOF-8 cluster (lowest energy of the system) are shown in Figure 7 where it can be seen that the ethylene and the ethane positions, relative to the IRMOF-8 cluster, are not similar for the same adsorption site. The interaction of the gas molecules with the IRMOF-8 cluster was calculated for all equilibrium systems in Figure 7. This interaction energy ($U_{interaction}$) was computed from eq 4:

$$U_{interaction} = U_{complex} - U_{adsorbate} - U_{cluster} \quad (4)$$

where $U_{cluster}$, $U_{adsorbate}$, and $U_{complex}$ correspond to the energies of the optimized cluster, the free adsorbate (ethylene or ethane), and the adsorbed molecule on the cluster surface, respectively.

The results for $U_{interaction}$ (Table 2) show that the adsorption site 2 corresponds to the more energetic one. Nevertheless, both molecules present almost the same interaction energy on this site. On the contrary, for adsorption sites 1 and 3, the interaction energy of ethane is about 3 kJ/mol lower than that for ethylene, which means that the interaction is stronger for the ethane molecule than for ethylene. This result is in agreement with the experimental data in Figure 3, because ethane is more adsorbed at low pressures (<600 kPa) than ethylene. Apparently, the result from adsorption site 2 is not significantly reflected on the experimental results, most

Table 2. Interaction Energies ($U_{interaction}$) of the Adsorbates with the IRMOF-8 Cluster on Adsorption Sites 1−3

adsorption site	adsorbate	interaction energy (kJ/mol)
1	ethylene	−13
	ethane	−17
2	ethylene	−35
	ethane	−35
3	ethylene	−15
	ethane	−18

probably because this site is a small spot that is filled when one molecule is adsorbed (i.e., small adsorption capacity).

Literature shows that ethane can be more energetically adsorbed than ethylene, for instance, on graphitized carbon.[32] The new interesting feature presented in this work is that this is also the case for IRMOF-8, which, unlike other MOFs, has neither unsaturated metal centers nor acidic groups that could develop enhanced interactions with the ethylene double bond, but, instead, has linkers that have two adjacent aromatic rings and that seem to be responsible for the enhanced interaction with ethane.

4. CONCLUSION

In summary, we have shown that the metal−organic framework IRMOF-8 presents higher adsorbed amounts of ethane than of ethylene in a wide range of pressures, near ambient temperature. This is one of the few cases where preferential adsorption of ethane over ethylene is reported and the selectivity values range between 3.4 and 1.6 depending on the temperature and pressure. Separation of mixtures was achieved in flow experiments, giving the desired higher retention for ethane, allowing ethylene to be obtained first out of the column. According to the results of the interactions energies, the differences in interactions of ethane and ethylene with the two adjacent aromatic rings in IRMOF-8 seem to play an important role in the results observed for the selective adsorption.

■ ASSOCIATED CONTENT

Supporting Information

Diagram of the volumetric apparatus, IRMOF-8 structure, FTIR data, thermogravimetric analysis, powder X-ray diffraction data, virial coefficients, and Henry constants. This material is available free of charge via the Internet at http://pubs.acs.org.

■ AUTHOR INFORMATION

Corresponding Author

*E-mail: jpsilva@fc.ul.pt.

Present Address

[§]School of Environment and Natural Resources (SENR), Doon University, Kedarpur, Dehradun-248 001, Uttarakhand, India.

Notes

The authors declare no competing financial interest.

■ ACKNOWLEDGMENTS

We acknowledge the financial help from Fundação para a Ciência e Technologia (FCT; Portugal) to CQB and strategic project PEst-OE/QUI/UI0612/2013. M.L.P. acknowledges the IF contract IF/00993/2012/CP0172/CT0013 and FEDER, QREN, COMPETE for funding PEst-C/CTM/LA0011/2013.

■ REFERENCES

(1) Lloyd, L. *Handbook of Industrial Catalysts*; Springer: New York, 2011.
(2) Sami, M.; Hatch, L. F. *Chemistry of Petrochemical Processes*; Gulf Publishing Co.: Houston, 2000.
(3) Jing, G.; Xianghong, W.; Shuhong, J.; Qian, Z.; Danxing, Z. Vapor-Liquid Equilibrium of Ethylene+Mesitylene System and Process Simulation for Ethylene Recovery. *Chin. J. Chem. Eng.* **2011**, *19*, 543−548.
(4) van Miltenburg, A.; Zhu, W.; Kapteijn, F.; Moulijn, J. A. Adsorptive Separation of Light Olefin/Paraffin Mixtures. *Chem. Eng. Res. Des.* **2006**, *84*, 350−354.
(5) Ruthven, D. M. Past Progress and Future Challenges in Adsorption Research. *Ind. Eng. Chem. Res.* **2000**, *39*, 2127−2131.
(6) Yang, R. T. *Adsorbents: Fundamentals and Applications*; John Wiley & Sons, Inc.: Hoboken, 2003.
(7) Gücüyener, C.; van den Bergh, J.; Gascon, J.; Kapteijn, F. Ethane/Ethene Separation Turned on Its Head: Selective Ethane Adsorption on the Metal-Organic Framework ZIF-7 through a Gate-Opening Mechanism. *J. Am. Chem. Soc.* **2010**, *132*, 17704−17706.
(8) Silva, F. A.; Rodrigues, A. E. Propylene/Propane Separation by Vacuum Swing Adsorption Using 13X Zeolite. *AIChE J.* **2001**, *47*, 341−357.
(9) van den Bergh, J.; Gucuyener, C.; Pidko, E. A.; Hensen, E. J. M.; Gascon, J.; Kapteijn, F. Understanding the Anomalous Alkane Selectivity of ZIF-7 in the Separation of Light Alkane/Alkene Mixtures. *Chem.—Eur. J.* **2011**, *17*, 8832−8840.
(10) Saini, V. K.; Andrade, M.; Pinto, M. L.; Carvalho, A. P.; Pires, J. How the Adsorption Properties Get Changed When Going From SBA-15 to its CMK-3 Carbon Replica. *Sep. Purif. Technol.* **2010**, *75*, 366−376.
(11) Olson, D. H.; Camblor, M. A.; Villaescusa, L. A.; Kuehl, G. H. Light Hydrocarbon Sorption Properties of Pure Silica Si-CHA and ITQ-3 and High Silica ZSM-58. *Microporous Mesoporous Mater.* **2004**, *67*, 27−33.
(12) Do, D. D.; Do, H. D. Cooperative and Competitive Adsorption of Ethylene, Ethane, Nitrogen and Argon on Graphitized Carbon Black and in Slit Pores. *Adsorption* **2005**, *11*, 35−50.
(13) Kroon, M. C.; Vega, L. F. *Langmuir* **2009**, *25*, 2148−2152.
(14) Böhme, U.; Barth, B.; Paula, C.; Kuhnt, A.; Schwieger, W.; Mundstock, A.; Caro, J.; Hartmann, M. Ethene/Ethane and Propene/Propane Separation via the Olefin and Paraffin Selective Metal-Organic Framework Adsorbents CPO-27 and ZIF-8. *Langmuir* **2013**, *29*, 8592−8592.
(15) Bux, H.; Chmelik, C.; Krishna, R.; Caro, J. Ethene/Ethane Separation by the MOF Membrane ZIF-8: Molecular Correlation of Permeation, Adsorption, Diffusion. *J. Membr. Sci.* **2011**, *369*, 284−289.
(16) MacGillivray, L. R. *Metal-Organic Frameworks: Design and Application*; John Wiley & Sons, Inc.: Hoboken, 2010.
(17) Sayaka, R. E.; Nakamura, S.; Ogasawara, Y.; Kurosawa, N.; Mizuno, N. Selective Sorption of Olefins by Halogen-Substituted Macrocation-Polyoxometalate Porous Ionic Crystals. *Chem. Mater.* **2012**, *24*, 325−33.
(18) Meek, S. T.; Greathouse, J. A.; Allendorf, M. D. Metal-Organic Frameworks: A Rapidly Growing Class of Versatile Nanoporous Materials. *Adv. Mater.* **2011**, *23*, 249−267.
(19) Rowsell, J. L. C.; Yaghi, O. M. Metal-Organic Frameworks: a New Class of Porous Materials. *Microporous Mesoporous Mater.* **2004**, *73*, 3−14.
(20) Mueller, U.; Schubert, M.; Teich, F.; Puetter, H.; Schierle-Arndt, K.; Pastre, J. Metal-Organic Frameworks - Prospective Industrial Applications. *J. Mater. Chem.* **2006**, *16*, 626−636.
(21) Eddaoudi, M.; Kim, J.; Rosi, N.; Vodak, D.; Wachter, J.; O'Keeffe, M.; Yaghi, O. M. Systematic Design of Pore Size and Functionality in Isoreticular MOFs and Their Application in Methane Storage. *Science* **2002**, *295*, 469−472.
(22) Orefuwa, S. A.; Yang, H.; Goudy, A. J. Rapid Solvothermal Synthesis of an Isoreticular Metal−Organic Framework with

Permanent Porosity for Hydrogen Storage. *Microporous Mesoporous Mater.* **2012**, *153*, 88−93.
(23) Myers, A. L. Equation of State for Adsorption of Gases and Their Mixtures in Porous Materials. *Adsorption* **2003**, *9*, 9−16.
(24) Pinto, M. L.; Pires, J.; Rocha, J. Porous Materials Prepared from Clays for the Upgrade of Landfill Gas. *J. Phys. Chem. C* **2008**, *112*, 14394−14402.
(25) Pires, J.; Saini, V. K.; Pinto, M. L. Studies on Selective Adsorption of Biogas Components on Pillared Clays: Approach for Biogas Improvement. *Environ. Sci. Technol.* **2008**, *42*, 8727−8732.
(26) Sircar, S.; Myers, A. L. A Thermodynamic Consistency Test for Adsorption From Binary Liquid Mixtures on Solids. *AIChE J.* **1971**, *17*, 186−190.
(27) Frisch, M. J.; Trucks, G. W.; Schlegel, H. B.; Scuseria, G. E.; Robb, M. A.; Cheeseman, J. R.; Montgomery, J. A., Jr.; Vreven, T.; Kudin, K. N.; Burant, J. C.; Millam, J. M.; Iyengar, S. S.; Tomasi, J.; Barone, V.; Mennucci, B.; Cossi, M.; Scalmani, G.; Rega, N.; Petersson, G. A.; Nakatsuji, H.; Hada, M.; Ehara, M.; Toyota, K.; Fukuda, R.; Hasegawa, J.; Ishida, M.; Nakajima, T.; Honda, Y.; Kitao, O.; Nakai, H.; Klene, M.; Li, X.; Knox, J. E.; Hratchian, H. P.; Cross, J. B.; Bakken, V.; Adamo, C.; Jaramillo, J.; Gomperts, R.; Stratmann, R. E.; Yazyev, O.; Austin, A. J.; Cammi, R.; Pomelli, C.; Ochterski, J. W.; Ayala, P. Y.; Morokuma, K.; Voth, G. A.; Salvador, P.; Dannenberg, J. J.; Zakrzewski, V. G.; Dapprich, S.; Daniels, A. D.; Strain, M. C.; Farkas, O.; Malick, D. K.; Rabuck, A. D.; Raghavachari, K.; Foresman, J. B.; Ortiz, J. V.; Cui, Q.; Baboul, A. G.; Clifford, S.; Cioslowski, J.; Stefanov, B. B.; Liu, G.; Liashenko, A.; Piskorz, P.; Komaromi, I.; Martin, R. L.; Fox, D. J.; Keith, T.; Al-Laham, M. A.; Peng, C. Y.; Nanayakkara, A.; Challacombe, M.; Gill, P. M. W.; Johnson, B.; Chen, W.; Wong, M. W.; Gonzalez, C.; Pople, J. A. *Gaussian 03*, revision B.03; Gaussian, Inc.: Wallingford, CT, 2003.
(28) Zhao, Y.; Truhlar, D. G. The M06 Suite of Density Functionals for Main Group Thermochemistry, Thermochemical Kinetics, Noncovalent Interactions, Excited States, and Transition Elements: Two New Functionals and Systematic Testing of Four M06-Class Functionals and 12 other Functionals. *Theor. Chem. Acc.* **2008**, *120*, 215−241.
(29) Zhao, Y.; Truhlar, D. G. Comparative DFT Study of van der Waals Complexes: Rare-Gas Dimers, Alkaline-Earth Dimers, Zinc Dimer, and Zinc-Rare-Gas Dimers. *J. Phys. Chem. A* **2006**, *110*, 5121−5129.
(30) Lazar, P.; Karlický, F.; Jurečka, P.; Kocman, M.; Otyepková, E.; Šafářová, K.; Otyepka, M. Adsorption of Small Organic Molecules on Graphene. *J. Am. Chem. Soc.* **2013**, *135*, 6372−6377.
(31) Feldblyum, J. I.; Wong-Foy, A. G.; Matzger, A. J. Non-Interpenetrated IRMOF-8: Synthesis, Activation, and Gas Sorption. *Chem. Commun.* **2012**, *48*, 9828−9830.
(32) Do, D. D.; Do, H. D. Effects of Potential Models on the Adsorption of Ethane and Ethylene on Graphitized Thermal Carbon Black. Study of Two-Dimensional Critical Temperature and Isosteric Heat versus Loading. *Langmuir* **2004**, *20*, 10889−10899.